



How Gulf-Stream SST-fronts influence Atlantic winter storms

Results from a downscaling experiment with HARMONIE to the role of modified latent heat fluxes and low-level baroclinicity

Hylke de Vries¹ · Sebastian Scher² · Rein Haarsma¹ · Sybren Drijfhout^{1,3} · Aarnout van Delden⁴

Received: 23 February 2018 / Accepted: 5 October 2018 / Published online: 12 October 2018
© Springer-Verlag GmbH Germany, part of Springer Nature 2018

Abstract

The strong horizontal gradients in sea surface temperature (SST) of the Atlantic Gulf Stream exert a detectable influence on extratropical cyclones propagating across the region. This is shown in a sensitivity experiment where 24 winter storms taken from ERA-Interim are simulated with HARMONIE at 10-km resolution. Each storm is simulated twice. First, using observed SST (REF). In the second simulation a smoothed SST is offered (SMTH), while lateral and upper-level boundary conditions are unmodified. Each storm pair propagates approximately along the same track, however their intensities (as measured by maximal near-surface wind speed or 850-hPa relative vorticity) differ up to $\pm 25\%$. A 30-member ensemble created for one of the storms shows that on a single-storm level the response is systematic rather than random. To explain the broad response in storm strength, we show that the SST-adjustment modifies two environmental parameters: surface latent heat flux (LHF) and low-level baroclinicity (B). LHF influences storms by modifying diabatic heating and boundary-layer processes such as vertical mixing. The position of each storm's track relative to the SST-front is important. South of the SST-front the smoothing leads to lower SST, reduced LHF and storms with generally weaker maximum near-surface winds. North of the SST-front the increased LHF tend to enhance the winds, but the accompanying changes in baroclinicity are not necessarily favourable. Together these mechanisms explain up to 80% of the variability in the near-surface maximal wind speed change. Because the mechanisms are less effective in explaining more dynamics-oriented indicators like 850 hPa relative vorticity, we hypothesise that part of the wind-speed change is related to adjustment of the boundary-layer processes in response to the LHF and B changes.

Keywords Atlantic winter storms · Gulf Stream · SST-fronts

✉ Hylke de Vries
hylke.de.vries@knmi.nl

Sebastian Scher
sebastian.scher@misu.su.se

Rein Haarsma
rein.haarsma@knmi.nl

Sybren Drijfhout
sybren.drijfhout@knmi.nl

Aarnout van Delden
a.j.vandelden@uu.nl

¹ Royal Netherlands Meteorological Institute, De Bilt, The Netherlands

² Meteorological Institute and Bolin Centre for Climate Research, Stockholm University, Stockholm, Sweden

³ University of Southampton, Southampton, UK

⁴ IMAU, Utrecht University, Utrecht, The Netherlands

1 Introduction

The Gulf Stream in the western North Atlantic ocean is a region characterised by strong contrasts in sea-surface temperature (SST), following the juxtaposition of a northward protruding tongue of warm surface waters and a narrow coastal bound region with cold waters. This region is also one of the worlds major genesis regions of mid-latitude storms and their subsequent intensification. It has long been put forward that this coalescence of the storm genesis region with the Gulf Stream is more than accidental. Considerable research has been conducted on the role of the ocean in explosive cyclogenesis (e.g. Sanders and Gyakum 1980; Anthes et al. 1983; Roebber 1989a, b; Kuo et al. 1991; Sheldon et al. 2016). Indeed, these studies show that cyclone development occurs more often in the vicinity of the

strongest SST-gradients and strong latent heat fluxes appear essential to explain the occurrence of very strong storms above sea (Roebber and Schumann 2011). Yet examining this role of the SSTs in storm intensification from a climatological perspective is hampered by the large natural variability in the atmospheric conditions that favour cyclogenesis, and by the fact that storm development is not caused by a single mechanism. In most of the region the background flow exhibits a strong vertical windshear following the equator to pole temperature gradient, and is therefore fundamentally unstable to small disturbances. Therefore most cases of cyclogenesis involve a more than fair amount of the classic cyclogenesis mechanism, baroclinic instability (e.g. Eady 1949; Petterssen and Smebye 1971; Sanders 1986; Methven et al. 2005). Theory and observational evidence suggests that surface heating and diabatic effects may substantially enhance the development further (Kuo et al. 1991; Davis et al. 1993; Moore and Montgomery 2004; Vries et al. 2010).

Several studies have been conducted on the climate impacts of the structure of the SST pattern of the Gulf Stream. For example, it has been shown to have a clear imprint on the atmosphere aloft, even at higher altitudes within the troposphere (Minobe et al. 2008). The presence of the Gulf Stream significantly impacts local precipitation and even the storm track (Minobe et al. 2008; Small et al. 2014). This implies that modelling the storm track with climate models will be compromised if the spatial resolution of the ocean and atmosphere is not sufficient to resolve the details of the Gulf Stream region, including the SST-front (Piazza et al. 2015; Scher et al. 2017). In addition, remote impacts of small-scale oceanic features on precipitation have been shown, which are also affected by spatial resolution (Ma et al. 2015).

Case studies on individual storms have provided valuable insights into the mechanisms causing the influence of SST-gradients on storm development (e.g. Giordani and Caniaux 2001; Jacobs et al. 2008; Booth et al. 2012; Sheldon et al. 2016). There are indications that both the absolute values of SSTs and the magnitude of the SST-gradient influence storm-development, with the absolute SST values being the more important driver, and latent heat release playing an important role (e.g. Booth et al. 2010, 2012). However, to go beyond a single case study and unravel the role of the different intensification mechanisms in a climatological study is not an easy task. Roebber (1989a) states that "...if the deepening rates arise as a sum of processes, then no matter what the probability distributions of the separate processes may be, their sum will have a distribution that tends more and more towards Gaussian as the number of process components increase".

This study aims to narrow the gap between the climatological studies and those describing single cases. In a sensitivity experiment we downscale a relatively large number of

storms that have occurred over the region with a state of the art regional atmospheric model. In this controlled environment, we keep the large-scale conditions under which these historic storms developed fixed, but vary the underlying SST fields. Specifically we investigate the role of the presence of the sharp SST-gradients on the development, by explicitly removing them in a second simulation of the storm. In this way we can examine whether a "typical" response exists to the presence of a strong SST-gradient, and therefore whether insights obtained from single case studies can be representative for all (or the majority) of storms.

2 Methods

In this study we downscale a number of winter storms that travelled over the Gulf Stream region. Many storms passed over the region, but due to computational constraints we restricted our analysis to 24 storms. These were selected randomly from the ERA-Interim dataset (Dee et al. 2011) from the period 2006–2012. There was no specific reason for using this period, and the only selection criterium was that the storms crossed or travelled over the Gulf Stream. The downscaling is carried out with HARMONIE in climate mode, HCLIM-ALARO (HCLIM from here) as described in Lindstedt et al. (2015). HARMONIE is used routinely and operationally as an NWP model in a number of mostly European countries. Although HCLIM can be run at very high resolution and with non-hydrostatic dynamics, computational limitations motivated to run in hydrostatic mode at 10 km horizontal resolution, using ERA-Interim as boundaries. The start- and end dates of the simulations are given in the table in Appendix 1. Each storm is simulated twice, a reference run (REF) and a run (SMTH) where the underlying SST field is strongly smoothed (details follow below). The tracks and average SST field of all REF-storms are shown in Fig. 1. We have visually compared the HCLIM output to ERA-Interim and concluded that the REF storms were developing very similarly.

2.1 Removal of the SST-front

The REF and SMTH simulations use the same lateral boundary conditions, but different underlying SST-fields. The REF run uses the NOAA 0.25° daily Optimum Interpolation Sea Surface Temperature data set (Reynolds et al. 2007). The SMTH run uses the same SST-dataset, but with a smoothing algorithm applied. The smoothing algorithm first fills up land points with the latitudinal mean SST-values of the domain as pseudo-SSTs, and then applies a 3×3 grid-point smoother for 2000 times consecutively. This procedure effectively removes the Gulf Stream warm extension and the strong SST-gradients

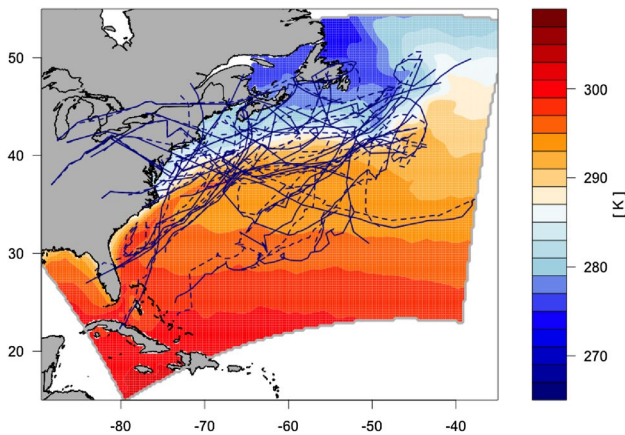


Fig. 1 Mean SST of all REF-storms (shading, units: K). Lines denote the tracks; REF (full) and SMTH (dashed). The simulation domain is outlined in grey

along the Gulf Stream front. The SST of SMTH is rescaled to have the same spatially average SST as REF, but still contains the large-scale meridional gradient of SST enforced by the boundary conditions.

Figure 2 shows the smoothed SST-field of all SMTH storms, and the absolute difference SMTH–REF, averaged over all cases. The difference pattern is a dipole of considerable amplitude, with increased SST north of the SST-front and decreased values south of it. The grey box outlines the HCLIM domain. It encompasses the region with the SST-front, but is still small enough to constrain the upper-level flow and large-scale baroclinicity by the boundaries. Indeed, the upper-level (above 500 hPa) flow and temperature structure are found to hardly differ between the REF and SMTH simulations.

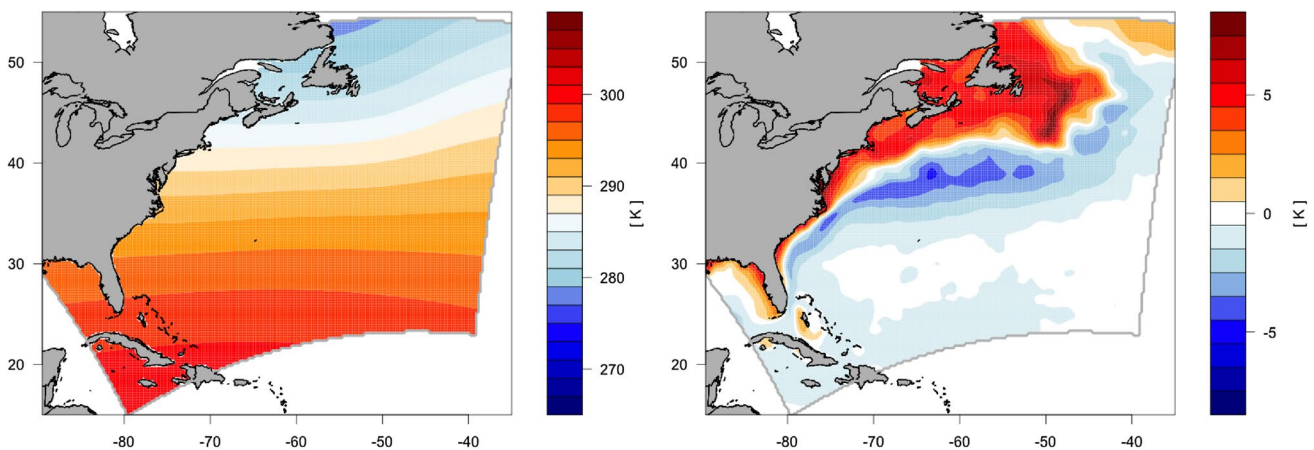


Fig. 2 As in Fig. 1 but for SST of SMTH (left) and the absolute difference SMTH–REF (right)

2.2 Along-track statistics

An along-track measure is developed to summarise the response of a chosen variable (e.g. wind speed) to the smoothing of the SSTs. First the center of the storm is identified as the local minimum of the geopotential at 925 hPa (ϕ_{925}) for every 6-hourly time step. This results in the track of the storm. The tracking is done for REF and SMTH separately, to account for deviations in the tracks. Generally these track-differences are small (Fig. 1), implying that the tracks are only weakly influenced by fine-scale details of the underlying SST pattern and more constrained by the lateral boundary conditions. Then the variable of interest is averaged over a square box around the center of the storm. This results in a single timeline for each variable. The size of the box is chosen to be rather small (30×30 km for ϕ_{925} , 100×100 km for all other variables) to focus on near-center storm response. Finally the timelines are time-averaged, yielding a single value for each simulation. Analyses are repeated for larger boxes (500×500 and 1000×1000 km) and systematic differences across scales will be discussed.

2.3 Single-storm ensemble

The tracks shown in Fig. 1 indicate a large variability in the simulated storms. Because each storm is simulated “only” twice, it is impossible to judge on a storm-by-storm basis whether the differences are significant. To alleviate this, we selected one storm (Storm 16) and constructed a 30-member ensemble for it. Member 0 is the REF storm. Members 1 to 10 are determined by using a linear combination of REF and SMTH, i.e., $SST_i = [(10 - i)SST_{ref} + (i)SST_{smth}]/10$ voor $i \in [0, 10]$. Members 11–20 are obtained using SST of REF augmented with a spatially non-correlated random perturbation field with an amplitude between ± 0.5 K. Finally, Members 21–30 are obtained by perturbing the SST of SMTH

using a randomly varying field. The random perturbations are different for each 6 h time-step. For the single-storm ensemble we analyse the storm-strength parameters in the same way as the other storms.

3 Results

3.1 Storm-strength changes

Figure 3 shows a histogram of the relative difference in mean along-track maximum 10-m windspeed (denoted W10X), which is our measure of storm strength. For this statistic we search in each 3-h time interval for the maximum 10-m windspeed within a box of 100×100 km around the track. These wind speeds are averaged along the track and compared. There is no sign of a systematic change. Instead, there are large variations, up to $\pm 25\%$ in the storm-strength response, as measured by this parameter. So both weakening and strengthening storms are found. Because the underlying SST-change is the only difference in boundary conditions, and because these differ substantially, depending on whether storms pass north or south of the original SST-front, we use colouring in the histogram to denote the mean absolute difference (SMTH–REF) in along-track SST. It appears that storms that meet on average cooler SST in SMTH (i.e., more southerly located tracks), tend to produce lower wind speeds, while those that experience on average warmer conditions show a more mixed picture. Thus storm-strength change and SST-change are correlated (Spearman rank correlation between relative windspeed difference and absolute SST difference is + 0.70). Similar results are found if we use

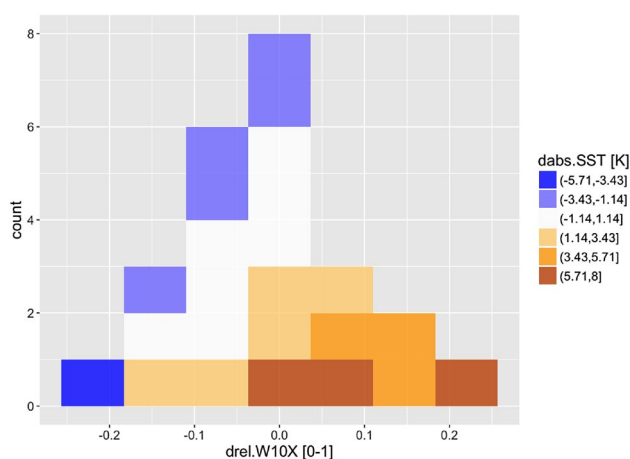


Fig. 3 Histogram of relative difference (SMTH–REF)/(REF) of the mean along-track 10-m wind speed maximum W10X. The maximum is computed using a window of 100×100 km around the track. The colouring denotes mean along-track absolute difference of SST (SMTH–REF)

sea-only points, increase the search-box to 500×500 , 1000×1000 km (not shown), or if we use as averaging period the time from the start of the simulation to the time of minimum in ϕ_{925} . Other storm-strength measures such as 850 hPa relative vorticity (zeta850), or the minimum in ϕ_{925} show a similar broad spread in the response (Fig. 9), with some storms getting weaker and some stronger. This mixed response is consistent with Roebber (1989a) who remarked that there is a tendency towards a Gaussian response if multiple mechanisms are acting simultaneously. From the large spread and the quasi-gaussian shape of the histogram, one could argue that from a statistical point of view there is simply no systematic response. However, we do not want to make that conclusion yet. Instead we will try to understand the reason underlying the mixed response.

3.2 Single-storm ensemble

To examine whether the response at the level of a single storm is significant, or at least systematic, we created an ensemble for a single storm (Storm 16 from the list). This storm travelled quite close to the SST-front and through the middle of the simulation domain. Figure 4 shows the time-series of a number of storm indicators for the ensemble, with color coding indicating the various groups within the ensemble. First of all, the tracks (top-left panel) are scattered closely around the tracks of REF (black) and SMTH (thick-red), except for two members (labelled 14 and 19) where the tracking failed. These two members are discarded from subsequent analysis. The SMTH-based members (thin-red) appear to propagate slightly further northward than the REF-based members, but we did not examine this aspect in detail. As expected, along-track average SST changes quite systematically as one cycles through the “linear-combination” members 1–10 (for the definition of the members, see Sect. 2.3) and is scattered around REF for members 11–20 and around SMTH for members 21–30. For 925 hPa-geopotential ϕ_{925} we had only 6-h output, and duplicated the points to 3 h (bottom-left). It shows gradual changes for members 1–10 and a clear separation of the REF-based and SMTH-based. A similar result holds for the variations in the wind-speed (bottom-right). These gradual, but systematic changes seen in especially members 1–10, and the clear separation of the two other groups (REF-based and SMTH-based), increase our confidence that the responses we see in other parameters are indeed systematic, and not influenced too strongly by the chaotic nature of the flow.

3.3 Environmental storm parameters

We now turn from the single-storm ensemble to the pair-simulations of all storms. Removing the SST front results in predictable changes in two environmental parameters that

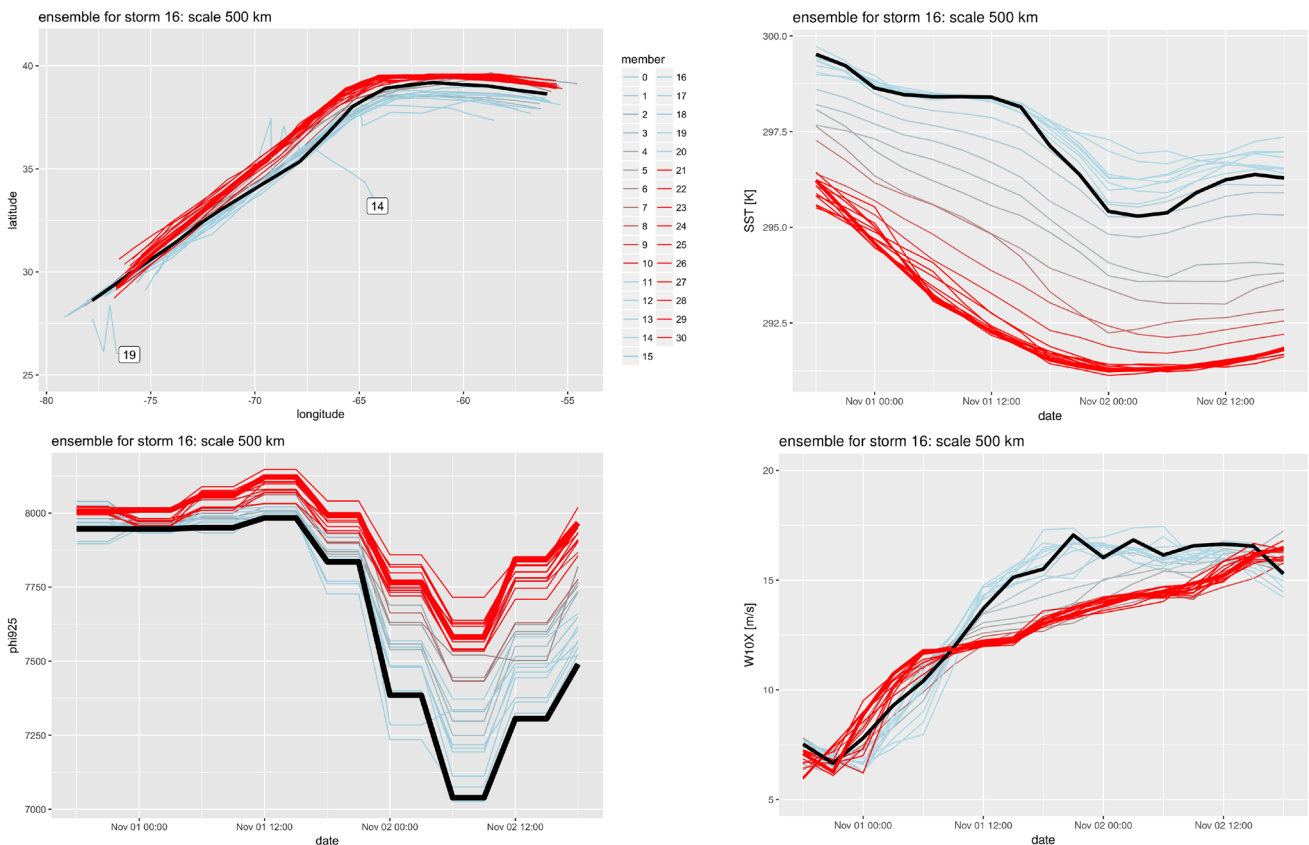


Fig. 4 Timeseries of various parameters for the mini-ensemble of storm 16. The thick black line denotes CTRL, the thick red line SMTH (the other members are explained in the text). Top row: tracks (left) and SST (right). Bottom row shows ϕ_{925} (left) and $wspdmax$ (right)

are known to be relevant extratropical storm development: (1) surface latent heat fluxes (LHF) and (2) low-level baroclinicity (B). LHF will influence the surface signature of storms by modifying boundary layer processes (e.g. vertical mixing) and may also influence cyclogenesis via the associated changes in diabatic heating. Low-level baroclinicity associated with strong horizontal temperature gradients and vertical stratification also plays a role in cyclogenesis. In addition to these two parameters the storms will be influenced and steered by the mid- to uppertropospheric flow configuration. The average vertical wind-shear of the troposphere determines to first order the maximal incipient cyclogenesis rate via the classic Eady and Charney mechanisms for baroclinic instability. However, by construction this part of the flow is largely kept constant for each storm-pair in our simulations.

Over the Gulf Stream, especially over the warm-tongue extension, the atmospheric air-temperature in the winter is generally lower than the SST underneath. This temperature contrast gives rise to considerable LHF from the sea to the air. The LHF peaks over the warm tongue, and strongly decreases northward due to the much colder SST (top-left panel, Fig. 5). LHF also decreases southward of the warm

tongue due to higher air temperatures. If the SST-front is absent or replaced by a longitudinal average (as approximately is the case in SMTH) LHF south of the front is much lower and north of it much higher. In the LHF-anomaly field, this becomes manifest as a dipole (bottom-left panel).

The second important difference between SMTH and REF is the change of low-level baroclinicity (B). Baroclinicity is crucial for storm development as it renders the basic flow inherently unstable to small disturbances. As discussed before, the upper-level flow is strongly constrained by the lateral boundary conditions, and will thus be quite similar for both REF and SMTH storms (i.e., they will still differ from storm to storm, but the SMTH-REF difference for a single storm case is small). Therefore it makes more sense to study the lower troposphere. We approximate the low-level baroclinicity by the absolute value of the horizontal temperature gradient at 850 hPa

$$B = |\nabla T|. \tag{1}$$

B is proportional to the vertical shear A of the wind and to the Eady (1949) growth rate. Averaged over all storms, B is positive everywhere in the domain for all levels up to the mid-troposphere, consistent with a northward decreasing

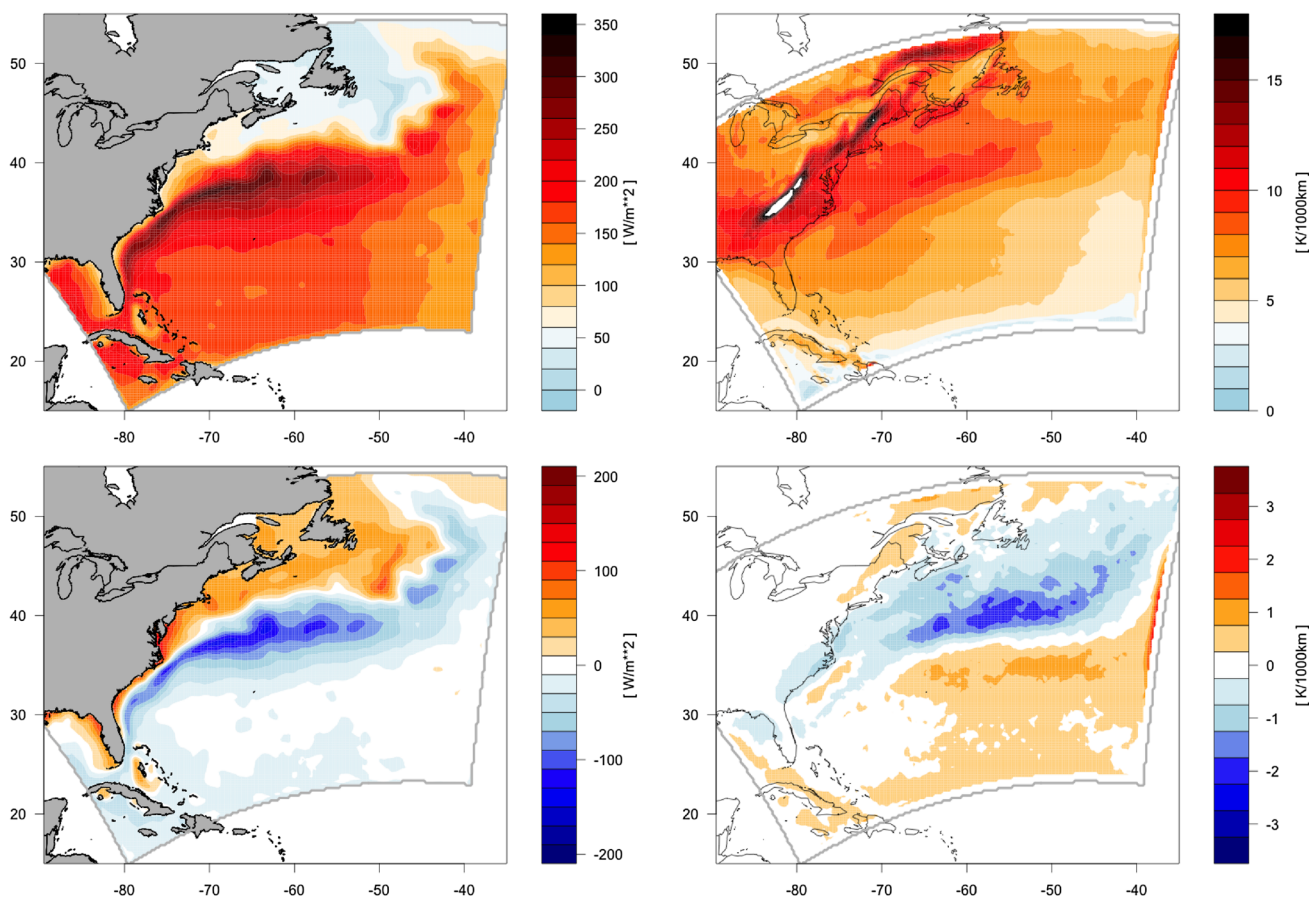


Fig. 5 Storm parameters. averaged over all simulations. Top-row: REF values for (left) surface latent heat flux and (right) absolute value of the horizontal temperature gradient at 850 hPa. Bottom row: absolute changes (SMTH-REF)

temperature and positive vertical wind shear. The top-right panel in Fig. 5 shows the average B (850 hPa) for all REF storms. The pattern is not uniform, with the largest amplitudes in the vicinity of the SST-front. The imprint of the underlying SST-front on B is much stronger at 925 hPa (Fig. 10 in Appendix 3), but also remains visible up to altitudes of 700 hPa (not shown). In the SMTH runs, the peak in amplitude of B is completely gone; low-level baroclinicity over the SST-front is therefore much less and we expect storms traveling over this region to be influenced by it. Meanwhile low-level baroclinicity in the adjacent sidebands is enhanced. The resulting anomaly field resembles a tripole (bottom-right panel). Again, at 925 hPa this is even more clear (Fig. 10).

Given these robust patterns of change in the storm parameters, the question is whether these can explain the differences in the storm-strength. Prior to answering this question let us first assess whether the two proposed parameters (so not their changes) do actually matter for the current set of REF-storms. Figure 6 shows a 2d-binned statistics plot of instantaneous W10X (scale: 100 km) of all REF-storms,

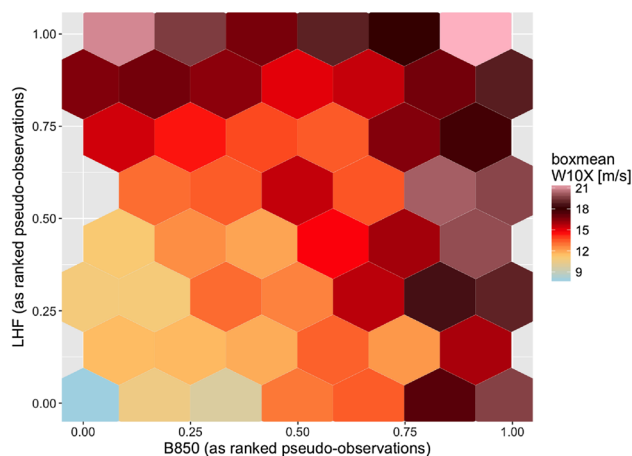


Fig. 6 2d-binned statistics of 3 h W10X using all REF-storms and all times (scale: 100 km). The storm parameters B (850 hPa) and LHF are used as coordinates. Each hexagon is coloured with the average W10X of all points within

where along-track LHF and B (850 hPa) are used as axes. For display purposes the B and LHF values are ranked first, such that the axes take the form of percentiles (lowest 10% B-values occur for $x < 0.1$, highest 10% LHF-values for $y > 0.9$ etc.). The figure shows that high W10X occur on average if either or both LHF and B are in their highest percentiles. The figure is qualitatively unaltered if we consider a larger storm-radius (using e.g. 500×500 km instead of 100×100 km), or if we adopt the standard definition of B in Eq. (1). Thus the results of Fig. 6 give us confidence that the two parameters LHF and B are indeed dynamically relevant for storms in the region.

Very similar results are found if we replace B by the full Eady index computed at 850 hPa (not shown). If we replace W10X by 850 hPa relative vorticity (zeta850), the pattern is however different (not shown). Similar to W10X, zeta850 is still generally higher when B or Eady is high, yet the relation with LHF is absent: strong and weak storms occur irrespective the amplitude of the underlying LHF.

3.4 Relating storm-strength changes to environmental parameters

Our final aim is to explain the variability in the storm-strength response seen in histogram Fig. 3. To this aim, we construct a very simple statistical model (MLM) where Δ LHF (the change of LHF) and ΔB (850 hPa) are used as predictors to explain the changes in mean along-track maximal

windspeed $\Delta W10X$. Here we want to focus on the phase where the rapid development occurs. Therefore we take the average value from the start of the simulation, up to the point where the storm reaches its along-track minimum in 925 hPa geopotential. In the MLM the following equation is solved using multiple least squares regression for the unknown regression coefficients a_i

$$\begin{aligned} \Delta W10X &= a_0 + a_1 \Delta LHF + a_2 \Delta B + \epsilon \\ &= \Delta W10X_{mlm} + \epsilon \end{aligned} \tag{2}$$

Here, $\Delta W10X$ denotes the change in storm strength and ϵ indicates the term from unexplained processes. Figure 7 (left) shows a scatter plot of the changes in the two storm parameters, with colour denoting the change in the storm-strength. They are uncorrelated, yet from the colouring it is obvious that the two, but especially LHF-change (like SST-change), can explain a substantial portion of the observed variance in storm-strength. Note that the values in the environmental parameters are different for each storm because (1) the tracks between the storms differ, (2) the precise location and amplitude of the SST-front differ for each simulation and (3) the storms occur at different dates, and thus SST and atmospheric conditions also differ for each storm.

The right panel of Fig. 7 summarises the performance of the MLM by means of a scatter plot between the true W10X changes and those predicted by the MLM. The (changes in the) two environmental parameters explain a large fraction of the observed changes in storm-strength: The Spearman

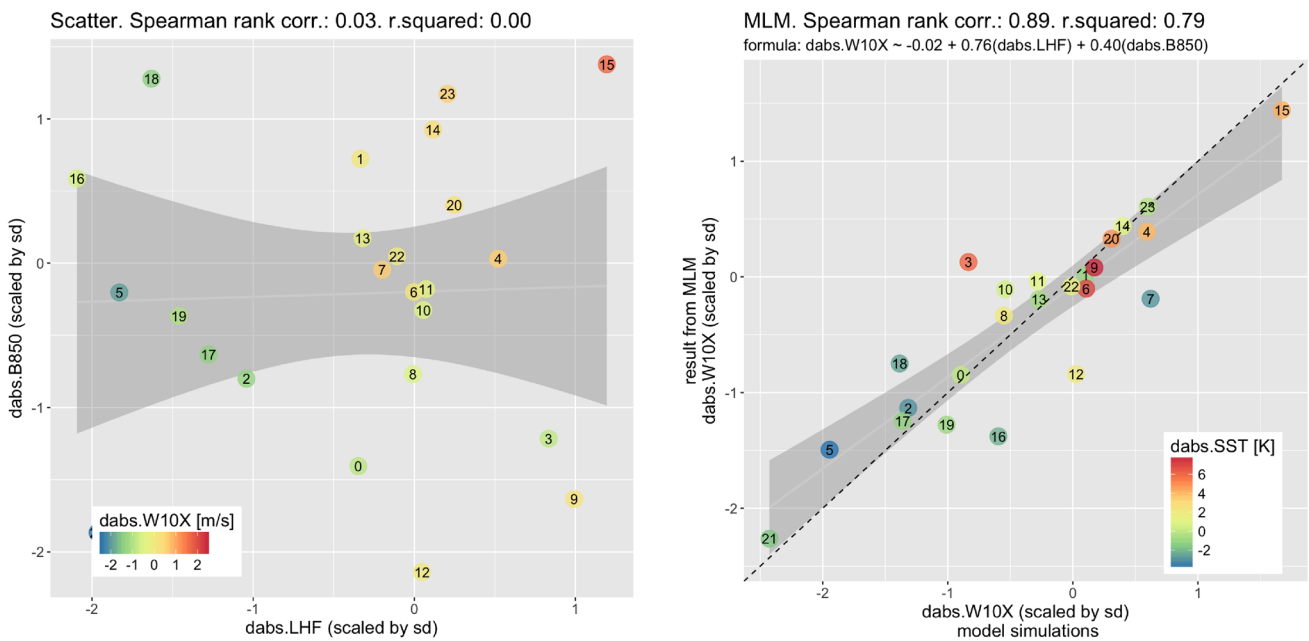


Fig. 7 (Left) scatter plot between the changes of the two environmental parameters. Colour denotes the change in W10X (m/s). (Right) performance of the linear statistical model that relates changes in

along-track W10X to changes of the environmental parameters. The grey regions indicate 95%-confidence bands of the linear fit between the variables on the x and y axes

rank correlation is 0.89 and the explained variance $r^2 = 0.79$. Since the changes in the two storm parameters are almost uncorrelated, their relative importance follows from the regression coefficients ($a_1 = 0.76$ and $a_2 = 0.40$). The most important contribution therefore comes from the latent heat flux mechanism. In addition, almost no offset is required ($a_0 = -0.02$) in the MLM, suggesting that we do not miss crucial mechanisms that systematically offset the results in a definite direction. A similar result, with a similarly high correlation near 0.90 is found if we use B (925 hPa) as a predictor instead of B (850 hPa). If we increase the horizontal scale (e.g. a box of 500 km) the explained variance is somewhat lower and this also occurs if we exclude land-points. Best results are then found if we use B at a higher level (e.g. at 700–500 hPa). If one replaces our measure of baroclinicity B by the full Eady index, the MLM results are almost the same.

In contrast to W10X, the changes of ZETA850 can less effectively be described using the two parameters. At 100 km scale, the LSM gives a Spearman correlation of 0.74 and an explained variance of just over 50% (not shown). At 500 km scale this even drops to very low values (correlation around 0.3), with no role played at all by LHF itself. Because the same two mechanisms are so much less effective in explaining the changes in relative vorticity at 850 hPa, we hypothesise that part of the near-surface wind-speed change is likely coming from the adjustment of the boundary-layer processes such as vertical mixing in response to the LHF and B changes.

Finally, we return to the single-storm ensemble. Applying the same techniques as above to that data set, we see that the drop in correlation is less if we move from W10X to ZETA850 (Fig. 8). For W10X again very high correlations are found (0.93), but even ZETA850 at 500 km scale remains reasonably well explained. Moreover, the single-storm results also stratify much better with the (along-track) SST-change itself (coloured dots), whereas this is not the case for the storm-pair simulations (Fig. 7). This must be due to the fact that the storms in the single-storm ensemble are much more similar to each other than those of the storm-pair simulations. In the latter the storm pairs differ strongly from each other in terms of for example timing of the year, direction of propagation across/along the Gulf Stream and the details of the atmospheric flow and even the underlying SST field.

4 Summary and concluding remarks

The presence of the SST-front over the Atlantic Gulf Stream influences storm development in the region. The SST-front does this by modifying two environmental parameters: near-surface latent heat fluxes (LHF), and low-level baroclinicity (B). While the LHF changes are caused by the large ocean-air temperature contrast, the low-level baroclinicity (visible up to 700 hPa in the simulations conducted in this study) is caused more indirectly, namely by

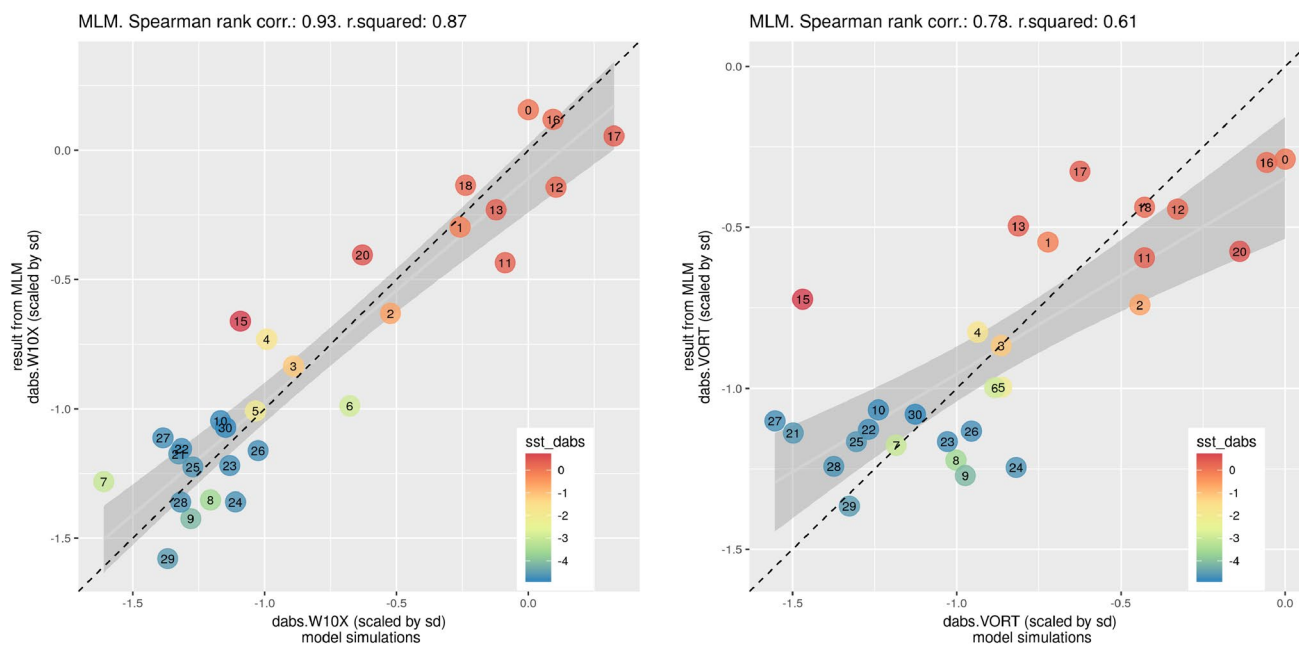


Fig. 8 Ensemble of storm 16. LSM to describe W10X changes (left) and ZETA850 changes (right) using LHF and B850 as drivers at 500 km scale

the presence of the strong horizontal SST-gradients that are so typical for the Gulf-Stream. Existing studies (e.g. Giordani and Caniaux 2001; Jacobs et al. 2008; Booth et al. 2012; Piazza et al. 2015; Sheldon et al. 2016) and the work of Roebber and Schumann (2011) have shown that surface heat fluxes and baroclinicity are important ingredients for storm development. LHF may exert an influence on near-surface wind speeds by modifying boundary layer processes such as vertical mixing of momentum and heat. Aloft it may influence cyclogenesis by modifying diabatic heating rates.

We downscaled 24 winter storms taken from ERA-Interim with HARMONIE, using either observed SST or a strongly smoothed SST, while keeping atmospheric boundary conditions unchanged. For each storm-pair thus created, the tracks are not influenced much by the presence of the front. However, differences in storm-strength show a large variability. Since the large-scale flow is constrained by the lateral boundaries, this variability must be caused by the differences in the boundary conditions the storms “see”. The most obvious factor is the difference in the SST along the track of the storm. Storms that pass north of the Gulf Stream SST-front experience warmer SSTs when applying smoothing, while storms south of the front experience colder SSTs. To satisfactorily explain the storm-strength differences, which can be as large as $\pm 25\%$, we studied how these SST differences impact the two above-mentioned processes. The first—the “Latent Heat Flux Mechanism”—directly communicates the SST-change to changes in LHF, which affects the development of the storms via latent heat release and changes of the stability of the atmosphere. This tends to cause a weakening of the storms if the average SSTs below the storm become lower, and a strengthening if the SSTs become higher through smoothing. The mechanism is in congruence with findings in Sheldon et al. (2016). Secondly it is shown that smoothing of SSTs affects the temperature structure of the atmosphere up to the mid-troposphere. Even though the domain of the experiment is rather small, the applied smoothing modifies the low-level baroclinicity. It is weakened in the central Gulf Stream region almost above the regions where the SST-gradients are largest, and slightly enhanced outside the central region. The final response of a storm follows from the combined effect of the two mechanisms. South of the Gulf Stream front, SSTs become colder when applying SST-smoothing, and both mechanisms work in the same direction and all storms weaken. North of the Gulf Stream front, SSTs become warmer when applying SST-smoothing, and the mechanisms work in opposite direction. In about half of these cases, the storms weaken, the other half strengthens. When combined in a simple

statistical model these two storm parameters can explain a large fraction of the storm-strength variability as measured by maximum near-surface wind speed (explained variance up to 80%). Because the changes in 850 hPa relative vorticity are less well explained in terms of the above mechanisms, we hypothesise that part of the near-surface wind-speed change is likely coming from the adjustment of the boundary-layer processes in response to the LHF and B-change.

We conclude with a few final remarks. By examining the differences in the highly controlled model environment, the present study is able to explain a large fraction of the storm-strength responses in terms of the two mechanisms. This should not be confused with the statement that these two mechanisms are the only ones determining explosive cyclogenesis over the region. To the contrary, large-scale baroclinicity and the natural variations thereof are probably the major development mechanism at hand. The essential point of our study is that we keep that aspect of the development constant for both REF and SMTH storms (case by case that is). Only in this way we can focus on the role of the other mechanisms related to the SST structure and gradients in modifying the storm development. The change in LHF is the most important factor of the two parameters, similar to findings in Booth et al. (2012), yet low-level baroclinicity adds considerably to the explained variance. Our results imply that a good representation of SST-fields, such as the Gulf Stream warm tongue, is necessary for correctly modelling storms, which has consequences for the accuracy of numerical weather prediction and climate simulations. A possible next research step would be to run a local coupled ocean-atmosphere model, which would also include potential feedback between the atmosphere and the ocean.

Acknowledgements This work has been funded by the PRIMAVERA project under Grant agreement 641727 in the European Commission’s Horizon 2020 research program. Author contribution statement: SS developed the initial ideas leading to this study; HdV and SS did the simulations and analyzed the data; HdV drafted the manuscript and all authors discussed the results and helped in improving the manuscript. The authors thank dr. James Booth, the reviewers and the editor for their constructive comments.

Appendix 1: Start and end dates of the simulations

The start and end-dates of the analysed storms are listed in the table below (format: yyyy-mm-dd, the storm-number is the indicator used e.g. in Fig. 7):

Start date	End date	Storm-number
2006-01-27	2006-02-01	20
2006-11-20	2006-11-26	21
2007-01-16	2007-01-25	00
2007-10-31	2007-11-06	22
2007-11-02	2007-11-11	01
2007-11-12	2007-11-24	02
2007-12-19	2007-12-29	03
2008-10-26	2008-11-06	04
2008-11-01	2008-11-07	23
2008-11-11	2008-11-22	05
2009-02-10	2009-02-20	06
2009-10-25	2009-11-03	07
2009-12-18	2009-12-30	08
2010-01-02	2010-01-13	09
2010-02-03	2010-02-15	10
2010-02-07	2010-02-19	11
2010-11-25	2010-12-04	12
2010-12-10	2010-12-21	13
2010-12-15	2010-12-26	14
2010-12-27	2011-01-08	15
2011-10-26	2011-11-05	16
2011-12-07	2011-12-17	17
2011-12-11	2011-12-20	18
2012-01-27	2012-02-08	19

Appendix 2: Relative vorticity at 850 hPa

Figure 9 shows the histogram of changes in relative vorticity at 850 hPa using a domain of 100 km centered around the track.

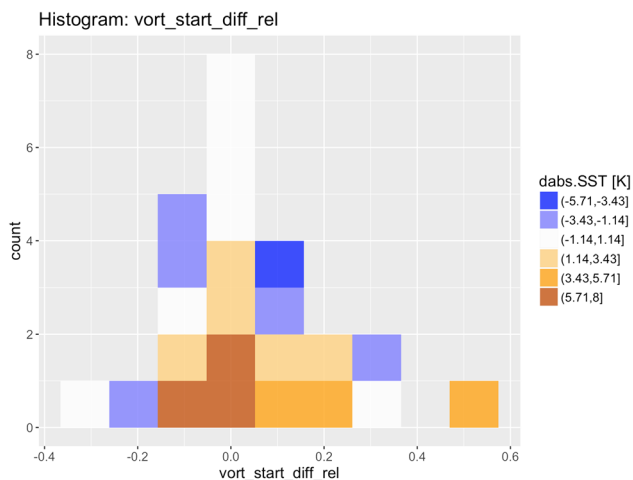


Fig. 9 As in Fig. 3 but for the relative vorticity at 850 hPa

Appendix 3: Absolute temperature gradient at 925 hPa

Figure 10 shows the absolute value of the horizontal temperature gradient at 925 hPa.

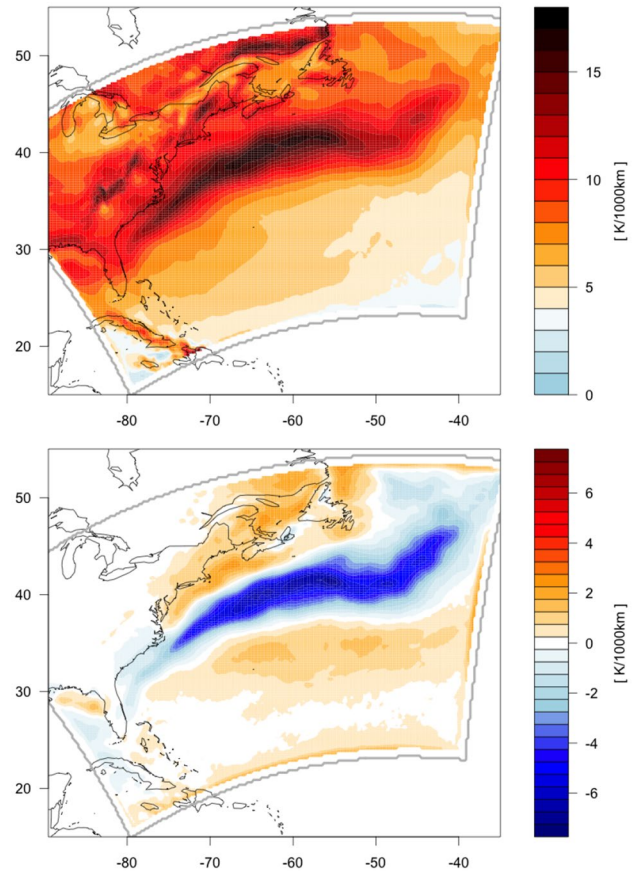


Fig. 10 As in Fig. 5 but for the absolute value of the horizontal temperature gradient at 925 hPa. Top: REF; bottom: absolute changes (SMTH-REF)

References

- Anthes RA, Kuo YH, Gyakum JR (1983) Numerical simulations of a case of explosive marine cyclogenesis. *Mon Weather Rev* 111:1174–1188. <https://doi.org/10.1175/1520-0493>
- Booth JF, Thompson L, Patoux J, Kelly KA, Dickinson S (2010) The signature of the midlatitude tropospheric storm tracks in the surface winds. *J Clim* 23(5):1160–1174. <https://doi.org/10.1175/2009JCLI3064.1>
- Booth JF, Thompson L, Patoux J, Kelly KA (2012) Sensitivity of midlatitude storm intensification to perturbations in the sea surface temperature near the Gulf Stream. *Mon Weather Rev* 140(4):1241–1256
- Davis CA, Stoelinga MT, Kuo YH (1993) The integrated effect of condensation in numerical simulations of extratropical cyclogenesis. *Mon Weather Rev* 121:2309–2330

- Dee DP, Uppala SM, Simmons AJ, Berrisford (2011) The ERA-Interim reanalysis: configuration and performance of the data assimilation system. *Q J R Meteorol Soc* 137(656):553–597. <https://doi.org/10.1002/qj.828>
- Eady ET (1949) Long waves and cyclone waves. *Tellus* 1:33–52
- Giordani H, Caniaux G (2001) Sensitivity of cyclogenesis to sea surface temperature in the Northwestern Atlantic. *Mon Weather Rev* 129(6):1273–1295
- Jacobs N, Raman S, Lackmann G, Childs P Jr (2008) The influence of the Gulf Stream induced SST gradients on the US East Coast winter storm of 24–25 January 2000. *Int J Remote Sens* 29(21):6145–6174
- Kuo YH, Low-Nam S, Reed RJ (1991) Effects of surface energy fluxes during the early development and rapid intensification stages of seven explosive cyclones in the Western Atlantic. *Mon Weather Rev* 119(2):457–476. <https://doi.org/10.1175/1520-0493>
- Kuo YH, Shapiro MA, Donall EG (1991b) The interaction between baroclinic and diabatic processes in a numerical simulation of a rapidly intensifying extratropical marine cyclone. *Mon Weather Rev* 119:368–384
- Lindstedt D, Lind P, Kjellström E, Jones C (2015) A new regional climate model operating at the meso-gamma scale: performance over Europe. *Tellus A* 67:24138
- Ma X, Chang P, Saravanan R, Montuoro R, Hsieh JS, Wu D, Lin X, Wu L, Jing Z (2015) Distant influence of Kuroshio eddies on north Pacific weather patterns? *Sci Rep* 5:17785
- Methven J, Hoskins BJ, Heifetz E, Bishop CH (2005) The counter-propagating Rossby-wave perspective on baroclinic instability. IV: Nonlinear life cycles. *Q J R Meteorol Soc* 131:1425–1440
- Minobe S, Kuwano-Yoshida A, Komori N, Xie SP, Small RJ (2008) Influence of the Gulf Stream on the troposphere. *Nature* 452(7184):206–209
- Moore RW, Montgomery MT (2004) Reexamining the dynamics of short-scale, diabatic Rossby waves and their role in midlatitude moist cyclogenesis. *J Atmos Sci* 61:754–768
- Petterssen S, Smebye S (1971) On the development of extratropical cyclones. *Q J R Meteorol Soc* 97:457–482
- Piazza M, Terray L, Boé J, Maisonnave E, Sanchez-Gomez E (2015) Influence of small-scale north atlantic sea surface temperature patterns on the marine boundary layer and free troposphere: a study using the atmospheric ARPEGE model. *Clim Dyn* 46:1–19
- Reynolds RW, Smith TM, Liu C, Chelton DB, Casey KS, Schlax MG (2007) Daily high-resolution-blended analyses for sea surface temperature. *J Clim* 20(22):5473–5496
- Roebber PJ (1989a) On the statistical analysis of cyclone deepening rates. *Mon Weather Rev* 117:2293–2298
- Roebber PJ (1989b) The role of surface heat and moisture fluxes associated with large-scale ocean current meanders in maritime cyclogenesis. *Mon Weather Rev* 117(8):1676–1694
- Roebber PJ, Schumann MR (2011) Physical processes governing the rapid deepening tail of maritime cyclogenesis. *Mon Weather Rev* 139(9):2776–2789
- Sanders F (1986) Explosive cyclogenesis in the west-central North Atlantic Ocean, 1981–84. Part I: composite structure and mean behavior. *Mon Weather Rev* 114(10):1781–1794. [https://doi.org/10.1175/1520-0493\(1986\)114](https://doi.org/10.1175/1520-0493(1986)114)
- Sanders F, Gyakum JR (1980) Synoptic-dynamic climatology of the Bomb. *Mon Weather Rev* 108(10):1589–1606
- Scher S, Haarsma RJ, de Vries H, Drijfhout SS, van Delden AJ (2017) Resolution dependence of extreme precipitation and deep convection over the Gulf Stream. *J Adv Model Earth Syst* 9:1186–1194. <https://doi.org/10.1002/2016MS000903>
- Sheldon L, Czaja A, Vanniere B, Morcrette C, Casado M, Smith D (2016) “A warm path” to gulf stream-troposphere interactions (**in preperation, personal communication**)
- Small RJ, Tomas RA, Bryan FO (2014) Storm track response to ocean fronts in a global high-resolution climate model. *Clim Dyn* 43(3–4):805–828
- de Vries H, Methven J, Frame THA, Hoskins BJ (2010) Baroclinic waves with parameterized effects of moisture interpreted using Rossby wave components. *J Atmos Sci* 67:2766–2784. <https://doi.org/10.1175/2010JAS3410.1>